Journal of Materials Chemistry A

Accepted Manuscript

ROYAL SOCIETY OF CHEMISTRY

www.rsc.org/materialsA

Journal Name

ARTICLE

O3-type Layered Transition Metal Oxide $Na(NiCoFeTi)_{1/4}O_2$ as a High Rate and Long Cycle Life Cathode Material for Sodium Ion Batteries

Received 00th January 20xx,
Accepted 00th January 20xx

DOI: 10.1039/x0xx00000x

www.rsc.org/

Ji-Li Yue, [a] Yong-Ning Zhou,*[b,c] Xiqian Yu,[c] Seong-Min Bak,[c] Xiao-Qing Yang*[c] and Zheng-Wen Fu*[a]

High rate capability and long cycle life are challenging goals for the development of room temperature sodium-ion batteries. Here we report a new single phase quaternary O3-type layer-structured transition metal oxide $Na(NiCoFeTi)_{1/4}O_2$ synthesized by a simple solid-state reaction as a new cathode material for sodium-ion batteries. It can deliver a reversible capacity of 90.6 mAh g^{-1} at a rate as high as 20C. At 5C, 75.0% of the initial specific capacity can be maintained after 400 cycles with a capacity-decay rate of 0.07% per cycle, demonstrating a superior long-term cyclability at high current density. X-ray diffraction and absorption characterizations revealed reversible phase transformations and electronic structural changes during the Na^+ deintercalation/intercalation process. Ni, Co and Fe ions contribute to the charge compensations during charge and discharge. Although Ti ions do not contribute to the charge transfer, it plays a very important role to stabilize the structure during charge and discharge by suppressing the Fe migration. In addition, Ti substitution can also smooth the charge-discharge plateaus effectively, which provides a potential advantage for the commercialization of this material for room temperature sodium-ion batteries.

Introduction

Sodium-ion batteries have attracted increasing attentions for large-scale energy storage applications because of the natural abundance of sodium resources and potential low cost. However, the lack of high performance cathode materials is one of the major obstacles for the development of current room temperature sodium ion batteries.[1-2] O3-type layer-structured materials $NaTMO_2$ (TM = transition metals) have been widely investigated as cathode materials for sodium ion batteries (SIBs) inspired by lithium battery system.[3-4] The commonly used 3d transition metals are Fe, Co, Ni, Mn, V, Cr and Ti. Among them, iron is the fourth most abundant element in the Earth's crust. Iron-based layer-structured materials attracted a lot of interests for SIBs applications.[5-9] Unlike electrochemical inactivity of $LiFeO_2$ for lithium batteries, $NaFeO_2$ is surprisingly electrochemically active with a discharge capacity of about 80 mAh g^{-1} when a cut-off voltage limit of 3.3 V vs Na^+/Na is used. Unfortunately, the structural deterioration of $NaFeO_2$ due to the Fe migration causes severe capacity fading within several cycles.[5] To address this issue, partial iron substitution by other transition metals in the layered $NaFeO_2$ structure, such as cobalt, manganese and nickel was considered and studied.[6-9] For example, Yoshida et al. synthesized O3-$NaFe_{1/2}Co_{1/2}O_2$ by solid state reaction. It yields a discharge capacity of about 160 mAh g^{-1} in an operating voltage range of 2.5-4.0 V.[6] O3-$NaFe_{1/2}Mn_{1/2}O_2$ delivers a capacity of 110 mAh g^{-1} in the potential range of 1.5-4.3V.[7] However, it suffered from nearly 20% capacity fading after 30 cycles at 0.05C, and the large polarization (~1 V) problem. The O3-$NaNi_{1/3}Fe_{1/3}Mn_{1/3}O_2$ cathode delivers a reversible capacity of about 100 mAh g^{-1} at 0.5C in a voltage range of 1.5 - 4.0 V.[8] Particularly, $NaNi_{1/3}Co_{1/3}Fe_{1/3}O_2$ delivers high capacities of 165 mAh g^{-1} at 0.1C and 80 mAh g^{-1} at 30C between 2.0 and 4.2 V,[9] but its galvanostatic charge-discharge curve displays multiple plateaus, indicating multiple phase transformations during cycling. It shows a 10% capacity fade after 20 cycles at 0.05 C. Recently, a complex O3-type layer-structured $NaNi_{1/4}Fe_{1/4}Co_{1/4}Mn_{1/4}O_2$ of four transition metal elements delivers a capacity of 183 mAh g^{-1} but shows an 11% capacity fading after 10 cycles at the current density of 0.1C was reported.[10] These results indicated that the substitution of Fe in $NaFeO_2$ with other transition metals is an effective way in changing the average working potential and tuning the electrochemical behaviour. They provided rich information on sodium electrochemistry of O3-type layer-structured materials and the possibility of using them as the cathode materials for SIBs. However, most of the studies mentioned above are using late transition metals which usually have more than 4 electrons in their 3d orbitals. Their 3d orbitals are quite localized due to the stronger core-electron interaction compared with the early transition metals (They usually have less than 4 electrons in their 3d orbitals). Previous research revealed that the early transition metal ions in

[a] Shanghai Key Laboratory of Molecular Catalysts and Innovative Materials, Department of Chemistry & Laser Chemistry Institute, Fudan University Shanghai, 200433, P.R. China. E-mail: zwfu@fudan.edu.cn
[b] Department of Materials Science, Fudan University, Shanghai, 200433, P.R. China. E-mail: ynzhou@fudan.edu.cn
[c] Department of Chemistry, Brookhaven National Laboratory, Upton, New York 11973, USA. E-mail: xyang@bnl.gov
† Footnotes relating to the title and/or authors should appear here.
Electronic Supplementary Information (ESI) available: [details of any supplementary information available should be included here]. See DOI: 10.1039/x0xx00000x

the layer-structured cathode materials had intrinsic capability to suppress the unit cell breathing range during cycling.[11] Doping the early transition metal in the layered compound may have some beneficial effects on the electrochemical behaviour by changing its local electronic structure. As one example of early transition metal substitution, Ti in layered $Li_1(Ni_xMn_xCo_{1-2x-y}Ti_y)O_2$ cathode for lithium ion batteries resulted in beneficial effects on reducing the structural distortions during delithiation and suppressing the formation of a secondary rock salt phase at high voltage charge.[12]

Here, we report a new quaternary O3-type layer-structured material of $Na(NiCoFeTi)_{1/4}O_2$ (denoted hereafter as NCFT) for the first time. Its electrochemical performance as a new cathode material for SIBs is evaluated in a sodium half-cell. Phase transition behaviours and electronic structural changes of NCFT during charge and discharge were investigated by X-ray diffraction and absorption techniques. It is demonstrated that this material has an impressive high rate capability and long cycle life for room temperature sodium ion batteries.

Experimental Section

Material Synthesis

O3-type $Na(NiCoFeTi)_{1/4}O_2$ (O3-NCFT) was synthesized by a conventional solid state reaction method. Na_2CO_3 (99.95% Alfa Aesar), TiO_2 (99.9% Sigma-Aldrich), Fe_2O_3 (99.99% Alfa Aesar), CoO (99.995% Alfa Aesar), and NiO (99.99% Sigma-Aldrich) are used as precursors in the mole ratio of 1.0:0.25:0.125:0.25:0.25. The precursors were mixed by a mortar and pestle, then the mixture was heated at 800 °C for 24 h in air.

Material Characterization

The morphology of the product was characterized by field mission scanning electron microscopy (SEM, Cambridge S-360). Powder X-ray diffraction (XRD) patterns were collected on an X-ray diffractometer (BrukerD8 Advance, Germany) with Cu-Kα radiation (λ = 0.1540 nm) at 40 kV, 40 mA. Data were obtained over the 2θ range of 10-80° for as-prepared materials and 10-70° for electrodes with a scan rate of 1° min^{-1}. XRD refinement was conducted by using the Rietveld method using GSAS program. High resolution transmission electron microscopy (HRTEM) and selected-area electron diffraction (SAED) were carried out on a JEOL JEM-2100F transmission electron microscope at an acceleration voltage of 200 kV. X-ray absorption spectroscopy (XAS) was performed at beamline 12BM of the Advanced Photon Source (APS) at Argonne National Laboratory and beamline BL2-2 of Stanford Synchrotron Radiation Lightsource (SSRL). Fe, Co, Ni, Ti K-edge XAS was collected in transmission mode. The XAS data was processed using Athena and Artemis software packages.[13-14]

Electrochemistry

The working electrode was prepared by spreading the slurry of 70 wt % O3-NCFT, 20 wt % carbon black, and 10 wt % polyvinylidenefluoride (PVDF, Sigma-Aldrich) onto the aluminum foil. The electrodes were dried at 120°C for 12 h, and punched to small circular pieces with a diameter of 14 mm. Electrochemical cells were assembled in an Ar-filled glovebox (MBraun, Germany). The electrolytes consisted of 1 M $NaClO_4$ (Alfa-Aesar) in a nonaqueous solution of ethylene carbonate (EC, Alfa-Aesar) and propylene carbonate (PC, Alfa-Aesar) with a volume ratio of 1:1, 5wt% fluroethylene carbonate (FEC) were added to prevent the electrolyte decomposition, according to the literatures.[15,16] Galvanostatic charge-discharge measurements were carried out at room temperature on a Land CT 2001A battery test system by using coin cells. The coin cell was assembled with pure sodium foil as the counter electrode, and a glass fiber (GB-100R, ADVANTEC Co., Japan) as the separator. The current densities and capacities of electrodes were calculated on the basis of the weight of active materials. For the cyclic voltammogram (CV) and Electrochemical impedance spectroscopy (EIS) test, the cells were constructed using the as-prepared material as working electrode and two sodium foils as the counter and reference electrode, respectively. CV tests were performed on electrochemical workstation CHI 660B in the potential range of 2.0 - 3.9 V vs. Na^+/Na at the scan rates of 0.1, 0.2, 0.5, 0.8 and 1.0 mV s^{-1}. EIS, with voltage amplitude of 5mV and frequency range of 10^5 Hz to 10 mHz, was used to evaluate the electrode processes at different temperatures.

Results and Discussion

Synthesis and Structural Characterization of O3-NNCFT

Single phase $Na(NiCoFeTi)_{1/4}O_2$ (NCFT) solid solution is prepared by a simple solid state reaction. X-ray diffraction (XRD) pattern of the synthesized NCFT is shown in Fig. 1a. All peaks can be well indexed to a hexagonal phase with space group of R-3m without impurity. The Rietveld refinement of the XRD pattern was carried out using the GSAS+EXPGUI suite [17, 18] based on the structure of α-$NaFeO_2$. As shown in Table S1, the lattice parameters of NCFT are a=b=2.976 Å and c=16.076 Å. These values are close to those of previous reported O3 type layer $NaMO_2$ (M=transition metal) oxides.[9, 10] The good agreement between the experimental pattern and the calculated one confirms the isostructure of NCFT with $NaFeO_2$, which is built by repeating sheets of TM-O_2 layer (TM = Ni, Co, Fe, Ti) with Na ions being coordinated octahedrally by oxygen (Fig. 1b). Scanning electron microscopy (SEM) image of synthesized O3-NCFT

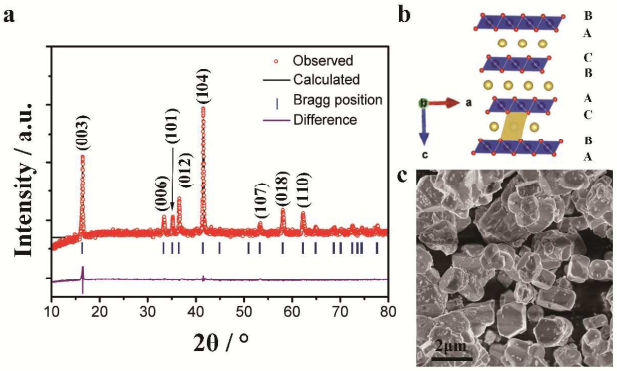

Fig. 1 (a) X-ray diffraction pattern and Rietveld refinement of the as-prepared O3-NCFT sample. (b) Schematic of the O3-NCFT crystal structure, legend: red, blue and yellow balls stand for oxygen, transition metal and sodium ions, respectively. (c) SEM image of the O3-NCFT material.

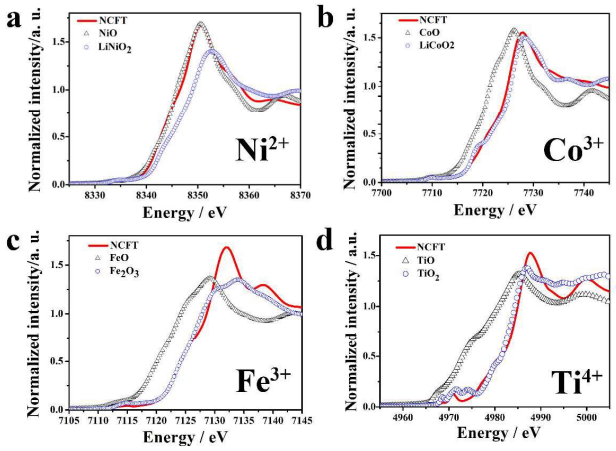

Fig. 2 XANES spectra at the (a) Ni, (b) Co, (c) Fe and (d) Ti K-edges of pristine NCFT and corresponding metal oxides references.

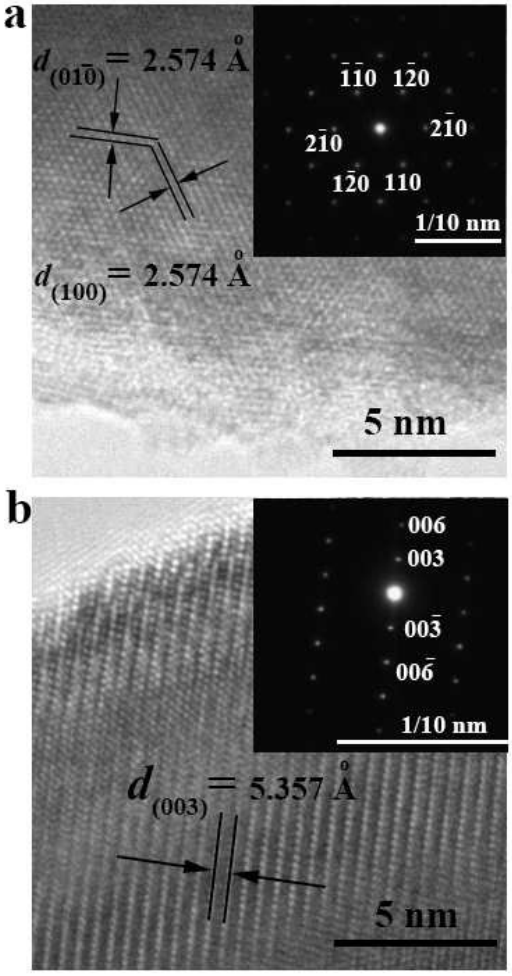

Fig. 3 HRTEM images and SAED patterns (insets) of the O3-NCFT material acquired from the (a) [001] and (b) [100] zone axis.

(Fig. 1c) shows the primary particles are in different shapes with sharp edges. The particle sizes are in the range of 1 ~ 3 μm.

Fig. 2a, b, c and d show the transition metal K-edge X-ray absorption near edge structure (XANES) spectra of the pristine NCFT. Comparing with the spectrum of the standard metal oxide compounds, we can estimate that the valence states of the Ni, Co, Fe, Ti ions in pristine NCFT are 2+, 3+, 3+ and 4+, respectively. The magnitudes of the Fourier transformed extended X-ray absorption fine structure (FT-EXAFS) spectra and their least square fits are plotted in Fig. S1. The first peak at R= ~1.7 Å is due to the contribution from the nearest TM–O_6 octahedra while the second peak at R= ~2.7 Å is attributed to the TM–TM_6 hexagon on the *a*–*b* plane in the second coordination shell. Structure parameters derived from the fitting are shown in Table S2. The different TM-O bond lengths for different transition metal elements agree well with the ion radii of the metal ions with the valence states determined by XANES.

To further reveal the structure of NFCT, high resolution transmission electron microscopy (HRTEM) and selected-area electron diffraction (SAED) measurements were performed. Fig. 3a and b show the TEM observation from [001] and [100] directions, respectively. In Fig. 3a, two dimension fringes have the same *d*-spacing of 2.574 Å, which can be attributed to the (010) and (100) planes. In Fig. 3b, the fringes with a *d*-spacing of 5.357 Å could be assigned to the (003) planes. The corresponding SAED patterns (insets of Fig. 3a and b) show perfect lattice structures, indicating a well crystallized structure of NFCT with a hexagonal symmetry. It is worth noting that [100] and [010] directions are favourable for the intercalation/deintercalation of Na ions into/from this structure.[19]

Electrochemical characterization

The galvanostatic curves of the O3-NCFT electrode cycled between 2.0-3.9 V vs. Na^+/Na at a current density of 12 mA g^{-1} are shown in Fig. 4a. The open circuit voltage (OCV) lies close to 2.8 V. In the initial charge process, a flat voltage plateau from 2.8 to 3.1 V is followed by a sloping voltage plateau from 3.1 to 3.9 V. The initial charge capacity is found to be 122 mAh g^{-1}, which corresponds to about 0.5 Na per NCFT. In the initial discharge process, a quite symmetric curve comparing with the charge process is observed. It includes a sloping region from 3.9 V to 2.9 V followed by a flat plateau at around 2.8 V. The initial discharge process yields a specific capacity of 116 mAh g^{-1}, which is about 95% of the initial charge capacity, indicating a quite high coulombic efficiency during the first cycle. In the subsequent cycles, the discharge curves are almost overlapped with the initial one, demonstrating the excellent reversibility. Comparing the electrochemical curves of O3-NCFT with that of the Fe-contained layer oxide reported in previous literatures $NaFe_{1/2}Co_{1/2}O_2$,[6] $NaFe_{1/2}Mn_{1/2}O_2$,[7] $NaNi_{1/3}Co_{1/3}Fe_{1/3}O_2$[9] and $NaNi_{1/4}Fe_{1/4}Co_{1/4}Mn_{1/4}O_2$,[10] in which multiple plateaus with larger steps are always involved, one can see that the smooth discharge and charge curves exhibit utterly different feature from the voltage profiles of the above compounds. Such different features could be resulted from the Ti substitution, which can tune the charge ordering property and reaction pathway effectively.[20] The moderate voltage feature of O3-NCFT is very beneficial for battery management and suitable for commercialization.

Fig. 4b shows the cyclic voltammogram (CV) curves of the O3-NCFT electrode between 2.0 and 3.9 V vs. Na^+/Na at a scan rate

of 0.1 mV s^{-1}. One pair of sharp anodic/cathodic peaks at 3.03/2.85V and a pair of broad peaks at 3.67/3.59V are observed in the first cycle. It was reported that the redox potentials of Ni^{2+}/Ni^{3+}, Co^{3+}/Co^{4+}, Fe^{3+}/Fe^{4+} and Ti^{3+}/Ti^{4+} in the layered oxide systems lie in the range of 2.5-3.8,[21,22] 3.5~3.7,[23] 3.2~3.5[24] and 0.6~1.6 V versus Na^+/Na [25], respectively. It could be reasonably assumed that the peak couple at 3.03/2.85 V correlate with the mainly redox reactions of Ni^{2+}/Ni^{3+}. The broad peak couple at 3.67/3.59V could be related to the redox reaction of Co^{3+}/Co^{4+} and Fe^{3+}/Fe^{4+}. The intensities and shapes of all anodic and cathodic peaks are maintained in the subsequent scans, indicating that the electrochemical process is highly reversible. These results are well in accordance with the galvanostatic charge-discharge curves.

The typical discharge curves of O3-NCFT at different C rates (C rate is calculated based on a specific capacity of 120 mAh g^{-1}) are shown in Fig. 4c. Specific capacities of 116.8, 114.7, 110.8, 108.6 and 101.9 mAh g^{-1} were obtained at the current densities of 0.1 C, 0.2C, 1C 2C and 5C, respectively. Even at 20 C, the material still can deliver a large discharge capacity of 90 mAh g^{-1} (about 78% of 0.1C rate). The cycle performance of this material at 1C, 2C and 5C rate

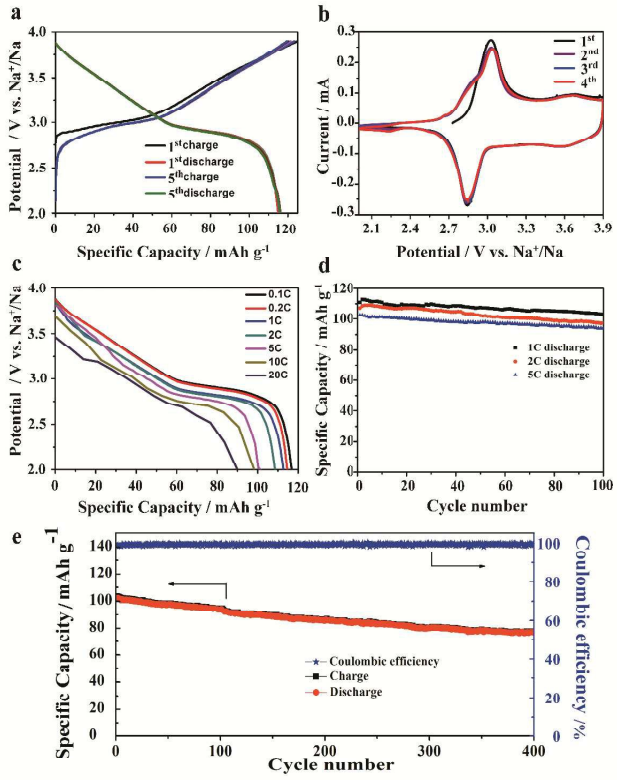

Fig. 4 (a) The galvanostatic charge/discharge curves of O3-NCFT in the initial five cycles at a current rate of 0.1C (12 mA g^{-1}) in the potential range of 2.0 - 3.9V versus Na^+/Na, (b) the initial four cyclic voltammograms of the O3-NCFT electrode between 2.0 and 3.9 V versus Na^+/Na at the scan rate of 0.1 mV s^{-1}, (c) Rate capability at various current rates, (d) Cyclic performances of the O3-NCFT electrode cycled at a current density of 1C, 2C and 5C. (e) Long term cyclic performances of the O3-NCFT electrode cycled at a current density 5C.

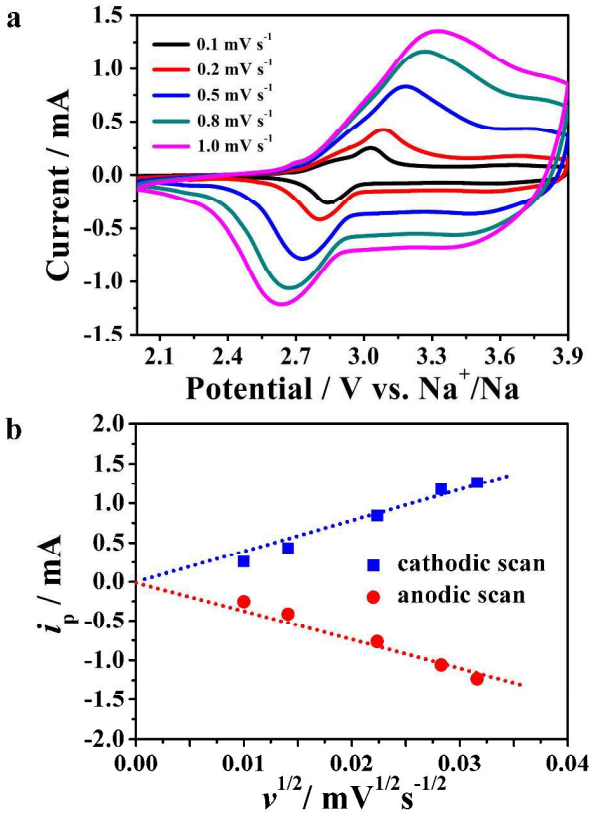

Fig. 5 (a) CV profiles at various scan rate of 0.1, 0.2, 0.5, 0.8 and 1 and mV s^{-1}. (b) Plot of peak current (i_p) as function of the square root of sweeping rates ($v^{1/2}$).

shown in Fig. 4d indicates that O3-NCFT electrode remain reversible capacities of 103.1, 97.2 and 94.1 mAh g^{-1} after 100 cycles, corresponding to a capacity retention of 93.1%, 89.5% and 92.3%, respectively. Fig. 4e shows the long-term cyclic performance at a rate of 5C. It can be seen that 75.0% of the initial specific capacity is maintained after 400 cycles at 5C with a capacity-decay rate of 0.07% per cycle, indicating a superior long-term cyclability.

The peak shape and peak current evolution of CV curves with sweep rates are related to the kinetics of Na intercalation/deintercalation in the O3-NCFT framework. Fig. 5a shows CV curves of O3-NCFT at various scan rates of 0.1, 0.2, 0.5, 0.8 and 1.0 mV s^{-1} in the potential ranges of 2.0-3.9 V. Along with the increased scan rates, the peak currents (i_p) of the oxidation and reduction peaks increase. The i_p can be plotted as a function of the scan rate $v^{1/2}$ for the cathodic and anodic processes. As shown in Fig. 5b, the peak currents i_p show a well linear dependence on the square root of the scan rate for both intercalation and deintercalation processes, indicating a diffusion-controlled behaviour. The diffusion coefficient (D) of Na^+ can be calculated according to the equation expressed as [26],

$$i_p = 2.69\times10^5 n^{3/2} A D^{1/2} v^{1/2} C_0 \qquad (1)$$

where n is the number of electrons per reaction species (1.0 for Na^+), A is the area of electrode (about 1 cm^2), D is the diffusion coefficient of Na^+, C_0 is the concentration of Na^+ in the lattice (i.e.,

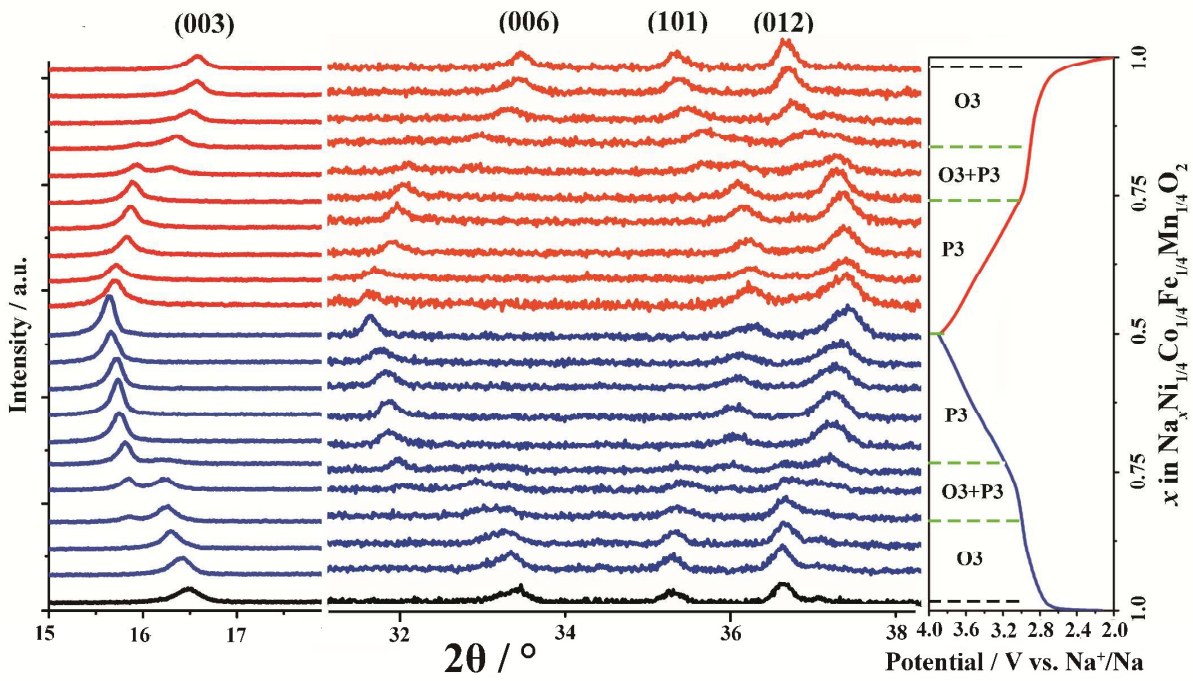

Fig. 6 Structure evolution of O3-NCFT during the electrochemical cycle. *Ex* situ X-ray diffraction patterns collected during the first charge/discharge of the Na/O3-NCFT cells under a current rate of C/10 at potential range between 2.0 and 3.9V. The corresponding charge-discharge profile is given on the right side of XRD patterns.

0.0404 mol cm^{-3}). The slope of the straight lines obtained from the plot of i_p versus $v^{1/2}$ are estimated to be 38.69 and -36.34 mA (mV s^{-1})$^{-1/2}$ for the intercalation and deintercalation processes respectively, and the calculated *D* values are obtained to be 1.64× 10^{-11} and 1.38×10^{-11} cm^2 s^{-1}, respectively. The activation energy of Na diffusion in Na(NiCoFeTi)$_{1/4}$O$_2$ is about 0.786 eV (Fig. S2). The high *D* values of O3-NCFT for Na ion diffusion should be responsible for the good reversibility, rate capability and cyclic performance of electrodes.

X-ray diffraction

To understand the structure evolution of the O3-NCFT during the Na$^+$ deintercalation/intercalation from the O3-NCFT host, XRD patterns were collected at a series depths of charge and discharge states, as shown in Fig. 6. The (003) and (006) peaks reflect the change of lattice parameter *c*, while (101) and (012) peaks mainly depend on the change of lattice parameter *a* and *b*. At the beginning of the charge, the (003) peak continuously shifted to the lower two-theta angles, indicating that a solid solution reaction was involved with *c*-axis expansion. As the Na ions were extracted, when *x*=0.85, a new (003) peak emerges, as we know, the (003) peak is a single-fold peak. Thus, every new (003) peak is a fingerprint for the formation of a new phase. Combining with other diffraction peaks, the new formed phase is resolved as a P3 stacking ordering. In the range of 0.85>*x*>0.75, two-phase coexistence could be observed. The intensity of the old (003) peak decreases and the new (003) peak increases with increasing Na-ion extraction, indicating a two-phase reaction. In the range of 0.75>*x*>0.5, the (003) peak of the pristine O3 phase disappears, and the (003) peak of the new formed P3 phase dominates. The (003) peak of P3 phase keeps shifting to lower two-theta angles, suggesting another solid-solution region. In the whole charge process, the (003) and (006) shift to the lower angles, while (101) and (102) shift to the high angles. This indicates that lattice parameter *c* increases while *a*(*b*) decreases. This is a typical unit cell breathing behaviour of the layer-structured cathode materials during charge. If the Na-ions are extracted further (*x*<0.5), the (003) peak will shift to higher 2ϑ angle (Fig. S3), indicating the collapse of the layered structure along *c* axis. This irreversible structure change will lead to severe capacity fading. During the discharge process 0.5<x<1, the phase transition behaviour follows an inversed way of the charge process. This reversible phase transition behaviour in the range of 0.5<x<1 are responsible for the excellent capacity retention.

X-ray absorption spectroscopy

To further investigate the local structures and valence state changes of Ni, Co, Fe and Ti of the O3-NCFT during charge and discharge, *ex* situ X-ray absorption spectroscopy studies at the Ni, Co, Fe and Ti K-edge were performed. Fig. 7a, c, e and g show the Ni, Co, Fe and Ti K-edge X-ray absorption near edge structure (XANES) spectra during the charge process, respectively. The charge/discharge curve and corresponding states where the XAS scans were taken are shown in Fig. S4. For the Ni K-edge (Fig. 7a), A rigid shift of the white line to high energy is observed, indicating the oxidation of Ni ions during Na extraction. The absorption edge at the end of the charged state is quite similar to the reference compound LiNiO$_2$, indicating the valance state of Ni in NCFT after 0.5 Na extracted is 3+. For Co and Fe (Fig. 7c and e), small shifts of the edge position to higher energy are observed. Compared with

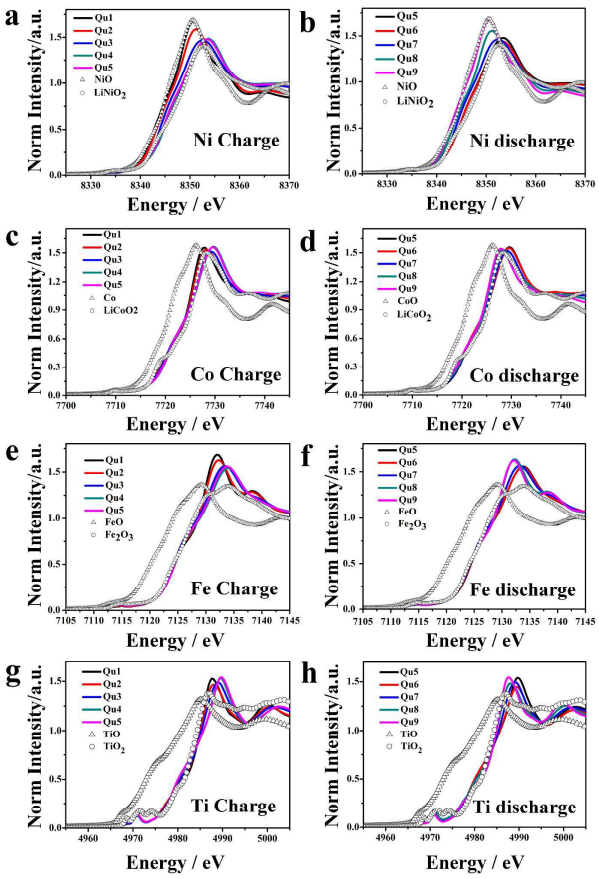

Fig. 7 (a), (c), (e) and (g) Normalized XANES of O3-NCFT at various stages during the first charge at Ni, Co, Fe, Ti K-edges, respectively, (b), (d), (f) and (h) Normalized XANES at various stages during the first discharge at Ni, Co, Fe, Ti K-edges, respectively. Qu1-Qu5 refer to the different states of charge process and Qu5-Qu9 refer to the different state of discharge process as shown by the red solid squares in Fig. S4.

the metal oxide reference spectrum, it can be estimated that the valence states of Co and Fe after charge are between 3+ and 4+. For Ti (Fig. 7g), the energy position of K-edge does not shift, but with little shape change. It is reasonable because the valance state of Ti is 4+ in the pristine NCFT. It is very hard to oxidize Ti^{4+} to a higher valence state. The little change of the edge shape indicates some local environment changes around Ti ions during the charge process. During the discharge process (Fig. 7b, d, f and h), all of the XANES spectrum for Ni, Co, Fe and Ti undergo opposite evolutions comparing to the charge process, and finally recover their pristine states, suggesting the reversible change of the electronic structure and surrounding environment of each transition metal ions in NCFT. In addition, the diffused Ti 3d orbitals can create strong Ti-TM interactions between two adjacent edge sharing TM-O_6 and Ti-O_6 octahedrals, so introducing Ti in this system might be able to suppress the Fe migration by changing the local electronic structures. This is quite beneficial for the long-term cycle performance of the Fe-contained layered cathode materials. The smooth charge-discharge curves could be a big advantage for the commercialization of this material for room temperature sodium-ion batteries.

Conclusions

In summary, we have successfully synthesized a new O3-type layer-structured metal oxide cathode $Na(NiCoFeTi)_{1/4}O_2$ for sodium ion batteries. It delivers a reversible capacity of 116 mAh g^{-1} in first cycle and has 93.03% capacity retention after 100 cycles at 1C rate. At a rate as high as 20C, a reversible capacity of 90.6 mAh g^{-1} can still be achieved. During 5C cycling, 75.0% of the initial specific capacity can be maintained after 400 cycles with a capacity-decay rate of 0.07% per cycle, indicating a superior long-term cyclability at high current density. The Ti substitution could smooth the charge/discharge plateaus effectively, and may contribute to the suppression of Fe migration. On the other hand, the synthesis method of this material is very facile and cost effective. Combining its high rate capability and long cycle life, NCFT could be a very promising cathode material for room temperature high power sodium-ion batteries.

Acknowledgements

This work was financially supported by the NSAF (Grant No.U1430104), 973 Program (no. 2011CB933300) of China, and Science & Technology Commission of Shanghai Municipality (08DZ2270500 and 11JC 1400500) and National Foundation of China (no. B1120132029). The work at Brookhaven National Laboratory was supported by the U.S. Department of Energy, the Assistant Secretary for Energy Efficiency and Renewable Energy, Office of Vehicle Technologies under Contract No. DE-SC0012704. We gratefully acknowledge the help by beamline scientists Sungsik Lee and Benjamin Reinhart at 12BM of Advanced Photon Source, a U.S. Department of Energy (DOE) Office of Science User Facility operated for the DOE Office of Science by Argonne National Laboratory under Contract No. DE-AC02-06CH11357. We thank technical supports by the beamline scientists from BL2-2 of the Stanford Synchrotron Radiation Lightsource, SLAC National Accelerator Laboratory, supported by the U.S. Department of Energy, Office of Science, Office of Basic Energy Sciences under Contract No. DE-AC02-76SF00515.

Notes and references

1 N. Yabuuchi, K. Kubota, M. Dahbi and S. Komaba, *Chem. Rev.*, 2014, **114**, 11636-11682.

2 D. Kundu, E. Talaie, V. Duffort and L. F. Nazar. *Angew. Chem. Int. Ed.*, 2015, **54**, 3431-3448.

3 K. Kubotu, N. Yabuuchi, H. Yoshida, M. Dahbi and S. Komaba, *MRS Bull.*, 2014, **39**, 416-422.

4 M. H. Han, E. Conzalo, G. Singh and T. Rojo, *Energy Environ. Sci.*, 2015, **8**, 81-102.

5 N. Yabuuchi, H. Yoshida and S. Komaba, *Electrochemistry*, 2012, **80**, 716-719.

6 H. Yoshida, N. Yabuuchi and S. Komaba, *Electrochem. Commun.*, 2013, **34**, 60-63.

7 N. Yabuuchi, M. Kajiyama, J. Iwatate, H. Nishikawa, S. Hitomi, R. Okuyama, R. Usui, Y. Yamada and S. Komaba, *Nat. Mater.*, 2012, **11**, 512-517.

8 D. Kim, E. Lee, M. Slater, W. Lu, S. Rood and C.S. Johnson, *Electrochem. Commun.*, 2012, **18**, 66-69.

9 P. Vassilaras, A. J. Toumar and G. Ceder, *Electrochem. Commun.*, 2014, **38**, 79-81.

10 X. Li, D. Wu, Y. N. Zhou, L. Liu, X. Q. Yang and G. Ceder, *Electrochem. Commun.*, 2014, **49**, 51-54.

11 Y. N. Zhou, J. Ma, E. Y. Hu, X. Q. Yu, L. Gu, K. W. Nam, L. Q. Chen, Z. X. Wang and X. Q. Yang, *Nat. Commun.*, 2014, **5**, 5381.

12 I. M. Markus, F. Lin, K. C. Kam, M. Asta and M. M. Doeff, *J. Phys. Chem. Lett.*, 2014, **5**, 3649-3655.

13 Newville, M. *J. Synchrotron Radiat.*, 2001, ***8***, 322-324.

14 B. Ravel and M. Newville, *J. Synchrotron Radiat.*, 2005, **12**, 537-541.

15 S. Komaba, T. Ishikawa, N. Yabuuchi, W. Murata, A. Ito and Y. Ohsawa, *ACS Appl. Mater. Interfaces*, 2011, **3**, 4165-4168.

16 B. Mortemard de Boisse, J. H. Cheng, D. Carlier, M. Guignard, C. J. Pan, S. Bordere, D. Filimonov, C. Drathen, E. Suard, B. J. Hwang, A. Wattiauxa and C. Delmas, *J. Mater. Chem. A*, 2015, **3**, 10976-10989.

17 A. C. Larson and R. B. Von Dreele, *General Structure Analysis System*, LANSCE, MS-H805, Los Alamos, New Mexico 1994.

18 B. H. Toby, *J. Appl. Crystallogr.*, 2001, **34**, 210-213.

19 S. Kim, X. H. Ma, S. P. Ong and G. Ceder, *Phys. Chem. Chem. Phys.*, 2012, **21**, 17147.

20 Y. S. Wang, J. Liu, B. Lee, R. Qiao, Z. Z. Yang, S. Y. Xu, X. Q. Yu, Y. S. Hu, W. L Yang, K. Kang, H. Li, X. Q. Yang, L. Q. Chen and X. J. Huang, *Nat. Commun.*, 2015, **6**, 6401.

21 S. M. Oh, S. T. Myung, J. Y. Hwang, B. Scrosati, K. Amine and Y. K. Sun, *Chem. Mater.*, 2014, **4**, 1620-1626.

22 S. Komaba, N. Yabuuchi, T. Nakayama, A. Ogata, T. Ishikawa and I. Nakai, *Inorg. Chem.*, 2012, **51**, 6211-6220.

23 D. D. Yuan, W. He, F. Pei, F. Y. Wu, Y. Wu, J. F Qian, Y. L. Cao, X. P. Ai and H. X. Yang, *J. Mater. Chem. A*, 2013, **1**, 3895-3899.

24 D. D. Yuan, Y. X. Wang, Y. L. Cao, X. P. Ai and H. X. Yang, *ACS Appl. Mater. Interfaces*, 2015, **7**, 8585-8591.

25 D. Wu, X. Li, B. Xu, N. Twu, L. Liu and G. Ceder. *Energy Environ. Sci.* 2015, **8**, 195-202.

26 A. J. Bard and L. R. Faulkner, *Electrochemical Methods: Fundamentals and Applications*, Willey, New York, 1980.

GRAPHICAL ABSTRACT

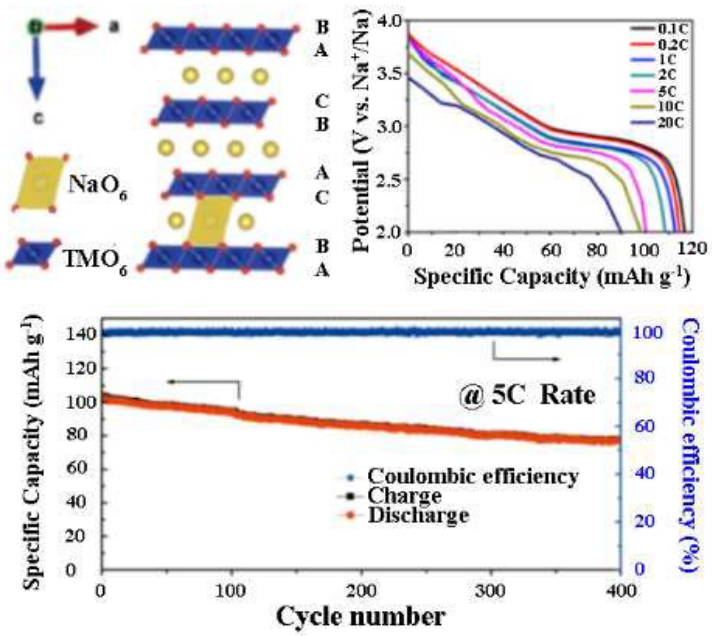

A new single phase quaternary O3-type layer-structured transition metal oxide $Na(NiCoFeTi)_{1/4}O_2$ was successfully synthesized. It can deliver a reversible capacity of 90.6 mAh g^{-1} at a rate as high as 20C. At 5C, 75.0% of the initial specific capacity can be maintained after 400 cycles with a capacity-decay rate of 0.07% per cycle.